AN ABSTRACT OF THE THESIS OF

Giang N. Ma for the degree of Master of Science in Chemical Engineering presented on March 10, 2004.
Title: XAFS Investigation of the Local Structure of Cadmium in $Cu(In_{0.7}Ga_{0.3})Se_2$ thin films

Abstract approved

Redacted for Privacy
Chih-hung Chang

We have performed fluorescence extended X-ray absorption fine structure (EXAFS) measurements on the Cd K-edge of partial electrolyte (PE) treated $Cu(In_{0.7}Ga_{0.3})Se_2$ (CIGS) thin film samples using synchrotron X-ray radiation. This data was compared to the EXAFS spectra of CdSe and CdO standards. Cd local structure models were constructed and used for the least square analysis of the spectra. The first model employed implantation of a cadmium atom and a single oxygen atom into the CIGS lattice. Specifically, an oxygen atom was introduced in the tetrahedral bonded Cd-Se local structure. Employing FEFF8 with WinXAS software package, experimental data was theoretically fitted to the first shell single-scattering paths of the Cd atom in the (PE) treated $Cu(In_{0.7}Ga_{0.3})Se_2$ thin film samples. The main peak observed in the data represents the Cd-Se bonds and the shoulder corresponds to the Cd-O bond. However, the number of total nearest neighbors is not consistent with this model. A two-phase model that includes both Cd-Se tetrahedron and Cd-O octahedron were then reconstructed. Again, a least-

agrees very well with the experimental data, and the total first nearest neighbor number is consistent with the two phase model at NN=4.2. This study indicates the surface of Cd partial electrolyte treated $Cu(In_{0.7}Ga_{0.3})Se_2$ thin films contains both CdSe and CdO.

XAFS Investigation of the Local Structure of Cadmium in $Cu(In_{0.7}Ga_{0.3})Se_2$ thin films

by
Giang N. Ma

A THESIS

submitted to

Oregon State University

in partial fulfillment of
the requirements for the
degree of

Master of Science

Presented March 10, 2004
Commencement June, 2004

Master of Science thesis of Giang N. Ma presented on March 10, 2004

APPROVED:

Redacted for Privacy

Major Professor, representing Chemical Engineering

Redacted for Privacy

Head of Department of Chemical Engineering

Redacted for Privacy

Dean of Graduate School

I understand that my thesis will become part of the permanent collection of Oregon State University libraries. My signature below authorized release of my thesis to any reader upon request.

Redacted for Privacy

Giang N. Ma, Author

ACKNOWLEDGEMENTS

I would like to take this opportunities to express my sincere appreciation to the following people:

- First, thank you to my devoted family, Mr. Giao N. Ma, my father, and Mrs. NgocThu Nguyen, my mother; who both always support and encourage me.
- Dr. Alex Chang, my advisor, for his valuable recommendations, guidance, and support throughout the research. Without his support, this thesis study could never been successful.
- Dr. Goran Jovanovic, Dr. William Warren, and Dr. Vanod Naranayan who were my committee members with their valuable help and suggestions in this thesis.
- All the professors in Chemical Engineering Department who provided me a indispensable motivation and knowledge during my course at Oregon State University.
- Doohyoung Lee who assisted in preparing for the oral presentation.
- Dr. Tomohiro Shabata and Dr. Soma Chattopadhyay from the MR-CAT at the APS beamline for their teaching and guidance during the experiments.
- To everyone in Dr. Chang's lab for their suggestions and help.
- To all my dear friends in the Chemical Engineering Department.
- This research has been supported by the National Renewal Energy Laboratory and the use of the APS beamline was funded by the U.S. Department of Energy.

TABLE OF CONTENTS

TABLE OF CONTENTS (Continued)

LIST OF TABLES

LIST OF FIGURES

LIST OF FIGURES (Continued)

XAFS Investigation of the Local Structure of Cadmium in $CuInSe_2$-Based Materials

Chapter 1

Introduction

Introduction:

High efficiency thin film $CuInSe_2$ (CIS) based solar cells have been widely demonstrated in laboratory scale devices (18.8%) and also in full size devices (12%). The crystal structure of CIS is shown in Figure 3.1.1.1. The yellow atoms represent copper, with the brown and gray atoms symbolize selenium and indium elements respectively.

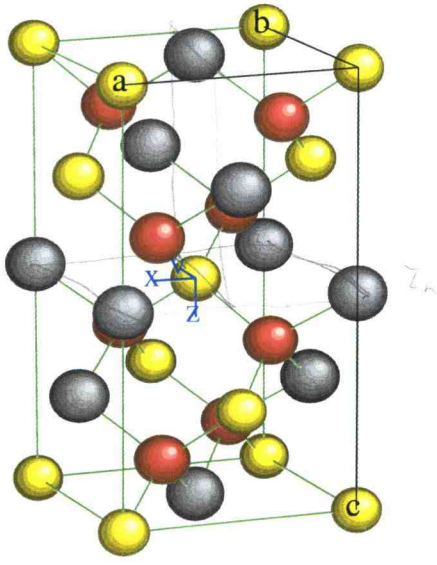

Figure 1.1: Chalcopyrite $CuInSe_2$ with space group I-42d (yellow as copper, red as selenium, and gray as indium).

The junction formation of the CIS thin film with a CdS layer formed during a chemical bath deposition (CBD) process is the critical step that plays an important role in the device functionality. In recent years, there have been considerable efforts directed

Author	Year	CBD Method	Instrumental Analysis	Model
Kessler et al.	1992	0.0015M $CdSO_4$, 1.5 M NH_3, 0.15 M thiourea	XPS and QMB	Graded Interface Distribution
Ramanathan et al.	1998	Cadmium Salt Partial Electrolyte (Cd PE) Treatment	XPS and SIMS	Type Conversion from p to n
Soo et al.	1999	0.0015M $CdSO_4$, 1.5 M NH_3, 0.15 M thiourea	ADXRF and XAFS	Cd neighbors around Cu

Table 1.1: Brief description of earlier research on CIS/CdS interfaces

toward explaining the mechanism for the CIS/CdS interface responsible for this dramatic improvement of the solar cell performance.

Ramanathan *et al.* have suggested that there is an ion exchange reaction at the near surface region of CIS absorbers with Cd or S ions, which chemically modifies the surface of the CIS device. Another study has proposed that Cd reacts with the absorber surface forming, or $CdIn_xSe_y$, which can produce a graded interface structure [Kessler, 1994]. More recently, Soo *et al.* has performed Cu *K-edge* EXAFS on CdS deposited $CuInSe_2$ single crystal samples. Their studies suggest the Cd atoms are sitting next to Cu atoms as first nearest neighbors based on least-square fitting of Cu-K EXAFS data. Table 1.1 illustrates the different methods used in these studies to elucidate the nature of the near interface junction of CIS absorbers and the CdS layer deposited by CBD.

To shed more light on this issue, we have studied the local structure of CIS/CdS interface using extended X-ray absorption fine structure (EXAFS) measurements performed on the Cd *K-edges*. The first-principles total energy calculations were also

quantitatively detail the local environment of the Cd ion in CIS thin films using least square analyses of EXAFS via different Cd local structure models.

We begin our report by describing the experimental details of the X-ray techniques used in our study in Chapter II. The data analysis procedures involving XAFS theory are given in Chapter III. The isolation of the main and shoulder peak contribution to the XAFS is presented in Chapter IV. Experimental results of detailed fits to the CIS/Cd interface are then discussed with a description of the mechanism of the Cd-diffusion into CIS thin films. Finally, a summary and the recommendation for future work will conclude this report.

Chapter 2

Literature Review

As a result of economical, political, and global concerns of the '70's and '80's over natural resources; there has been great impetus to develop cleaner alternative energy sources [S. Licht, 1997]. Solar energy remains the principal clean, abundant, renewable energy source available to us. Photopotentials used to directly convert sunlight into electrical energy have been widely studied since the first examinations by Becquerel in France in 1839 of the electrochemical phenomenon found in nature. The first solid-state photopotentials in 1876 consisted of a selenium device made by Adams and Day in England. Since then, there has been a variety of materials used, such as copper oxide, thallous sulfide, and silicon compounds.

Since the '90's, copper indium diselenide (CIS) thin films have been widely applied in new generations of high efficiency solar cell devices that employ CdS buffer layers [Herrero, 2000]. A fair amount of research has been done on this chalcopyrite material and its related compounds, such as $CuInGaSe_2$ (CIGS) based devices. Most studies preferred and utilized chemical bath deposition (CBD) process consisting of an aqueous solution of ammonia, cadmium salt, and thiourea to deposit the thin layer of CdS on top of the CIS substrate. Using sulphide ions as precipitating agents, the CBD process allows control of the homogenous precipitation of metal ions resulting in epitaxial growth in most samples. This interface quality between the CIS absorber and the CdS layer (CIS/CdS) is thought to be critical to the performance of the solar cell

device. Other deposition processes were initially developed, such as vacuum evaporation and sputtering techniques. However these alternative methods did not exhibit good deposition coverage and uniformity of the thin CdS layer.

This chapter is separated into three sections with respect to previous studies on the various proposed mechanisms of the interface formation between CIS/CdS junction through CBD treatments. All literature studies employed similar CBD recipes consisting of an aqueous solution containing ~0.0015 M $CdSO_4$, ~1-1.5 M NH_4OH, and ~0.15 M thiourea at 60-80°C for 10 minutes.

2.1 A Graded Distribution (J. Kessler 1992)

Kessler et al. studied the interfacial chemistry of CIS/CdS junction through CBD process in 1992 with X-ray photoelectron spectroscopy (XPS) and quartz crystal microbalance (QCM) analysis. Their research revealed that a *graded distribution* of CdSe and $CdIn_xSe_y$ layers are formed due to a strong initial reaction of the cadmium ions with the CIS surface during the CBD process. The deposition of occurs when the ionic product of both reagents exceeds the solubility product of the compound being deposited, known as the *ion-by-ion* mechanism. This ion exchange is suggested to occur between Cu atoms in the crystal lattice with Cd atoms in the presence of ammonia solution with dissolved Cd^{2+} ions [Nakada, 2000].

Using XPS analysis, the surface composition and the chemical states of CIS samples were characterized with different treatments of the CBD process. It revealed that samples treated with ammonia alone lead to a large loss of indium and oxides indicating

preferential etching of In^+ ions by the NH_3 [Herrero, 2000]. Copper and selenium signals relative to initial references were similar and showed little etching effects from the ammonia. However, a treatment of NH_3 with the addition Cd^{2+} ions shows different results. Nearly no copper was detected at the surface, while a large cadmium signal was observed from the energies of the Cd 3d photoelectrons and Cd Auger structures. These could not be determined to be either cadmium ions, CdO or $Cd(OH)_2$ alone, though. The indium signal again decreased, but was less than the ammonia alone experiment indicating a *blocking effect* of the indium etch due to the cadmium. The selenium signals remained consistent with the previous experiment with a different shape. The shift in the Se Auger signal can be explained by the formation of CdSe at the interface which is also confirmed by the Cd 3d binding energy.

Thermochemical calculations show that the solubilities of selenide pure phases ($CuInSe_2$, Cu_2Se, In_2Se_3) in ammonia are very low while the corresponding oxides are very soluble. This is evident in QCM studies by observing the loss of mass detected by the microbalance. Thus, indicating indium and oxides are being etched by the ammonia. Along with additions of thiourea (a reducing species) the loss of mass is stopped, which acts as a blocking effect and removes the dissolved oxygen. In the presence of Cd^{2+} ions, the mass loss is again noticed and suggests that an ion exchange between cadmium and indium in In_2Se_3 occurs; which then leads to CdSe,

$$In_2Se_3 + 3Cd(NH_3)_4^{2+} + 8OH^- \Leftrightarrow 3CdSe + 2InO_2^- + 12NH_3 + 4H_2O \qquad \textbf{(2.1.1)}$$

With a Gibbs energy of,

$$\Delta G = -279kj \cdot mol^{-1} \qquad \textbf{(2.2.2)}$$

In the case of CIS, the reaction is possible with indium if the stabilization energy with respect to binaries, Δ, is lower than 279 kJmol^{-1}. Also resulting in CdSe,

$$2CuInSe_2 + 3Cd(NH_3)_4^{2+} + 4OH^- \Leftrightarrow Cu_2Se + 3CdSe + 2InO_2^- + 12NH_3 + 2H_2O \quad \textbf{(2.2.3)}$$

Resulting in a Gibbs energy of,

$$\Delta G = -279 + \Delta kJ \cdot mol^{-1} \quad \textbf{(2.2.4)}$$

The chemical etching of the absorber surface is observed to be an important factor in CBD processes [Herrero, 2000]. Thiourea in excess amounts are also favorable for preparation of CIS/CIGS solar cells [D. Lincot, 1992]. Growth kinetics study indicate that the S/Cd ratio is much lower than that expected for CdS, which suggests CdSe growth.

2.2 Type Conversion from p to n (K. Ramanathan 1998)

For some time, the interface between the CIS absorber and the CdS layer was treated as an abrupt heterojunction. Studies by K. Ramanathan *et al.* [1998] has shown cadmium atoms introduced to such levels that a thin n-type emitter region can be formed at the CIS surface as a homogenous buried distribution. The in-diffusion of Cd^{2+} ions from the chemical bath solution into the top few nm of the CIGS surface has been analyzed through XPS. Secondary ion mass spectrometry (SIMS) was also used to determine the distribution of the elements in the polycrystalline films. The Cd atoms were hypothesized to form Cd_{Cu} vacancy defects, providing the required near-interface charge support for high efficiency device [Kronik, 2000].

Ramanathan *et al.* used similar partial electrolyte treatments as Kessler *et al.* The CIGS absorbers were subjected to Cd^{2+} ions and ammonium hydroxide. This *partial electrolyte* (PE) treatment was done to study the performance of devices without the CdS layer. Their device efficiencies were comparable to that of the best to that date. Group IIB elements are well known as n-type dopants in CIS/CIGS absorbers. From XPS analysis, there appears to be an increase in the Cd concentration in the front region, possibly to a depth of 500-1000 Å from the CIGS/CdS interface.

Diffusion in polycrystalline thin films can be quite aggressive through the grain boundaries, and it is important to sort out the contributions of intergrain and intragrain effects. SIMS confirmed that the in-diffusion of cadmium coincides with a slight depletion of copper levels in the front region. Analysis of the Cd 3d and Se 3d Auger lines demonstrate that the Cd is bound to Se, and the peak position can be assigned to the CdSe. The variations in the peak positions are due to the Cd diffusion at graded distributions.

The implications made here suggest that the wet chemistry in CBD enables devices to function like n^+p junctions with a very well matched lattice window layer that also acts as a shield to the CIGS absorber from further ZnO sputtering damage. The CBD process is a two-fold procedure, with the first step involving cadmium diffusion into the CIS layer through an ion-by-ion exchange; while a conversion from p to n type conduction change occurs in the absorber layer in the second step [Nakada, 2000]. The ion-exchange reaction is described as the out-diffusion of Cu coupled by the in-diffusion of Cd atoms. This extrinsic doping may play an important role in the formation of a

buried n-doped region, which supports the electric field of the device. Both are facilitated by the ability of the ammonia to complex the constituent ions. It is therefore possible for the copper deficient nature of the surfaces to present natural sites for the occupation by cadmium, presumably because of their very close ionic radii, 0.97 Å for Cd^{2+} and 0.96 Å for Cu^{2+} (Nakada *et. al.* 2001).

2.3 Occupation of Cadmium onto interstital sites next to Copper atoms (Y.L. Soo)

The work of Y.L. Soo et. al. [1999] investigated the interface morphology and migration of constituent atoms in single crystals of CIS/CdS heterojunctions. This was done through angular dependent X-ray fluorescence (ADXRF) and X-ray absorption fine structure (XAFS) measurements using hard X-rays from synchrotron radiation. Their results show that both Cu and Se atoms have migrated into the CdS layer in the heterojunction while In atoms remain intact in the $CuInSe_2$ single crystals.

ADXRF was used to investigate the depth distribution of Cu, Se, and In in pure CIS single crystals and in CIS/CdS heterojunctions. This technique is element specific and can help probe possible migration of the constituent atoms from the CIS absorber to the CdS layer. In ADXRF experiments, X-ray fluorescence pertaining to a selected element in the material is measured as a function of the X-ray penetration depth by varying the incidence angle of radiation. The angular dependence of total fluorescence yield (FY) can then be obtained. ADXRF curves show the onset of the In FY at ~0.08° is caused by a larger depth through which the incident X-ray beam has to penetrate in order to reach the In atoms in the buried CIS single crystal. These features are all expected for

a junction with a sharp interface and with constant In concentration profile in CIS. The gradual decrease of the copper and selenium FY at high angles is indicative of a concentration gradient, resulting from a redistribution of these atoms.

EXAFS was also used in this study to measure the Cu and Se K-edge of CIS/CdS samples using a standard fluorescence detector. Experimental curves are fitted with theoretical calculations using the coordination number and interatomic distances for CIS derived from XRD. These studies, by Ramanathan *et al.*, have clearly demonstrated that both Cu and Se atoms have migrated into the CdS (with an opposite introduction of Cd and O atoms into the absorber) layer in the heterojunction, while indium atoms remain intact in the $CuInSe_2$ single crystals.

Possible changes of the local environment around Cu and Se as a result of CdS coating on CIS have been studied using Cu and Se K-edge EXAFS. An additional small peak to the left of the main Cu K-edge peak is identified to be a new Cd neighbor shell around Cu with an average coordination number of 0.6 at a distance of 2.07 from the Cu atom. The Cu atoms have migrated from CIS into the CdS layer in the CIS/CdS junction and possibly form some Cu-Cd complexes therein, or the Cd atoms have diffused into the CIS and show up as new neighbors around Cu.

Chapter 3

Materials and Methods

3.1 Characteristics of $Cu(In,Ga)Se_2$/CdS and standard samples

3.1.1 CIGS Thin Film Deposition

The CIGS absorbers were grown at the National Renewal Energy Laboratories (NREL) by a three-stage process on ~1 mm thick soda-lime glass (SLG) substrates [Gabor, 1994]. A 1-μm thick layer of molybdenum (Mo) was initially deposited on the substrate through sputtering techniques, which serves as a backing electrode. Thin films of CIGS were made by co-evaporating the principal elements onto the Mo-coated SLG substrate in a Se atmosphere. The first step in this process involved the deposition of a $(In_xGa_{1-x})_2Se_3$ layer at 300°C on the substrate. This was followed by evaporation of Cu and Se at 550°C to make the film slightly Cu rich. The composition of the sample was restored to slightly In + Se rich by addition of $(In_xGa_{1-x})_2Se_3$ again. The Cu concentration in the near-surface region was carefully controlled so that the overall Cu/(In + Ga) ratio is less than unity. The substrate samples were rotated at 10 rpm in order to ensure a uniform film composition. High purity elements (99.9999%) were used as starting materials in this process. The resulting absorber material (sample reference #1852) was roughly 2.5 μm thick and was p-type with a hole density of $1\text{-}3x10^{16}\,cm^{-3}$. The nominal composition was determined to be $CuIn_{0.7}Ga_{0.3}Se_2$.

3.1.2 Cadmium Ion Doping of CIS absorber

The photovoltaic junction is generally completed by the deposition of a thin (~50 nm) CdS layer by CBD process as described in the literature review section employed in previous studies. Although the most efficient solar cell devices have been fabricated in this manner there are many drawbacks involving the CdS layer. It was found that the band gap of the CdS layer is low enough to limit the short wavelength part of the solar spectrum that can reach the absorber, which leads to reduction of the current efficiency [Johnson, 2002]. Also from a practical point of view, it would be beneficial to eliminate this layer to reduce the generation of large quantities of hazardous waste, such as the environmentally unfriendly Cd ions. Many groups are seeking alternative processes to the wet chemistry of CBD (i.e. vacuum techniques) to add simplicity to production, in lieu of alternating between vapor and wet process. However, the CBD process can be realized to be more commercially cost effective for large production set-ups.

In our study, an alternative process similar to that of CBD was used to study how the beneficial junctions between the CIS absorber were formed. This process, referred to as a Cd ion partial electrolyte (Cd PE) process, has previously yielded excellent working devices with CIS absorber layers [Ramanathan, 1998]. Devices made in this manner have had success in eliminating the CdS buffer layer by essentially only diffusing Cd ions into the absorber. This is done through the use of a chemical bath similar to that used to deposit the CdS layer with the exclusion of the sulfur-containing ingredient, thiourea. The bath composition was as follows: 0.0015 M and 1.5 M $CdCl_2$ with 1.5 M NH_4OH at

80°C for 10 minutes. The sample absorber referenced #1852 was treated to a low and high cadmium salt concentration to exaggerate the effects of dilute cadmium ion doping through elevated exposures to the Cd^{2+}. These are designated as the CIGS/Cd 0015PE sample and the CIGS/Cd 15PE sample in the results section.

3.1.3 CdO and CdSe Powder Standards

Similar to the thin film samples described above, fluorescent measurements of the Cd K-edge for the powder samples were performed in the same manner. These were used as reference samples for comparison analysis to the thin films. Powder standards of CdO and CdSe compounds were spread over a transparent tape, taking care to uniformly distribute the powder to avoid pinholes. Pure standard compounds of 99.9999% were purchased from Alfa Aesar.

In addition, $CdIn_2Se_4$ standards were prepared from powder CdSe and In_2Se_3 in boron nitride (BN) coated evacuated fused silica ampoules. The BN coating prevents devitirification of the fused silica ampoule at high temperatures [Shukri *et al.*, 1993]. These mixtures were then slowly heated to the melting temperature the gradually cooled to 700°C, and were kept in furnace at 700°C for a week to assure equilibrium was reached. The annealed mixture was then quenched cooled in liquid nitrogen. Powder XRD and wavelength dispersive X-ray spectroscopy were used to verify the formation of desired homogenous single-phase materials.

3.2 X-ray Absorption Fine Structure measurements

3.2.1 Experimental Setup

X-ray fluorescence measurements were performed on the Materials Research Collaborative Access Team (MR-CAT) beamline of the Advanced Photon Source (APS) at Argonne National Laboratory. A schematic diagram of the experimental setup is shown in Figure 3.2.1.1. Studies at the beamline use a set of standard procedures to assure data quality and experimental control. A checklist, abbreviated as H.A.L.O., was formulated by Bunker *et al.* that incorporates instrument and electronic preparation to ensure instrumental quality and reproducibility within the experiments being done. The abbreviation stands for *harmonics, alignment, linearity, and offset* of the electronics and beamline instruments that need are dealt with prior to examining samples.

The beamline used at the APS consists of an undulator A with optics incorporating a Si(111) double crystal monochromator, and a Pt coated harmonic-rejection mirror. This was set to reject the third order harmonics of the incident photons, which may cause non-linearity and background distortions within the collected data.

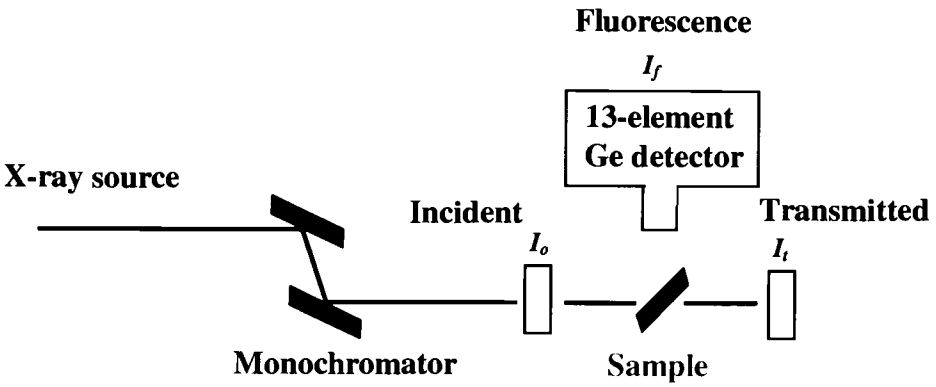

Figure 3.2.1.1: Schematic diagram of X-ray beamline setup

Thin film samples were measured using fluorescence data collected on a liquid nitrogen cooled multi-element germanium detector, while taped powdered samples were examined with a standard Lytle detector with an in flux of argon gas to allow ionization of third harmonic excitations. Both these samples were situated such that the incident X-ray beam is striking the sample surface at an angle of 45°. Clipping and blocking of the beam is checked to make sure alignment of the sample and reference signals to the detector is met. These X-ray fluorescence EXAFS spectra were measured at room temperature inside the experimental hutch. Dark currents were also measured and subtracted for offset of the electronic currents that may cause noise in the data. This done by measuring fluorescent signals with the shutter to the hutch closed so that no X-ray beam enters the detector. This allows only the electronic noise signals to be detected and subsequently deducted.

3.2.2 X-ray Fluorescence Multi-Channel Detector

X-ray fluorescent photon intensities from the irradiated thin film samples were monitored using a multi-channel detector placed at a 90° angle relative to the beam that is striking the sample at 45° (Figure 3.2.2.1). Multi-channel detectors allow for energy resolution that isolates Cd $K\alpha$, $K\beta$ peak signals, thus eliminating the need for background fluorescence removal from the raw data as seen in most single channel ionization counters. The energy resolving power of the Ge detectors can partially discriminate and remove Bragg spikes that occur from the incident beam energy. Such removal is accomplished by replacing the affected data by the normalized mean of the other

Figure 3.2.2.1: 13-element Ge Fluorescence Detector

channels. In this way, we can usually generate a full absorption spectrum over the energies of interest with small experimentally induced spikes or dips.

Besides the ability to resolve the Cd *Kα* fluorescence, the main utility in using the Ge detector is to maintain linearity of oscillations at energies far above the edge. Detector linearity is essential and is calibrated initially by holding the incident beam to the sample constant and varying the subsequent transmitted beam through the energy of interest.

3.3 Data Analysis

3.3.1 XAFS Theory

The application of hard X-rays from synchrotron radiation for structural and electronic characterization of a material has been implemented. Other X-ray investigation techniques, such as X-ray Diffraction (XRD), also reveals the *average* structure of solid material. However, these have difficulty in determining the local structure in disordered systems. X-ray Absorption Fine Structure (XAFS) can be used on all types of solid matter irrespective of the degree of crystallinity (Pandya, 1991). XAFS studies can be utilized in dilute samples such as doped thin films, whereas XRD techniques are generally employed to materials that have long-range structural order (i.e. bulk samples).

All matter absorbs X-rays through the photoelectric effect, which is electron excitation, and can be characterized by the absorption coefficient, $\mu(e)$. The absorption coefficient can be described by the intensity of an X-ray beam as it passes through a material of thickness dx as illustrated in Figure 3.3.1.1,

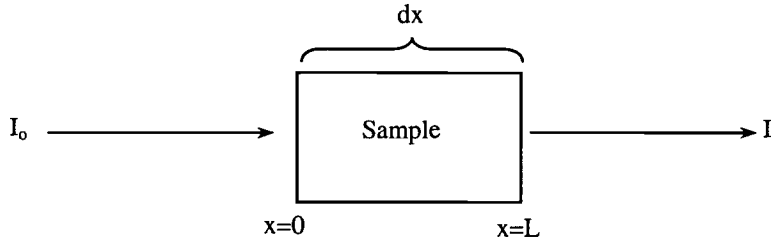

Figure 3.3.1.1: X-ray intensity passing through solid sample

The intensity of the incident photons, I_o, and the transmitted beam, I, can be expressed as a function of the thickness of sample, x,

$$\frac{dI}{dx} = -\mu(e) \bullet I \qquad (1)$$

where μ is the absorption coefficient and e is the X-ray photon energy. Integrating over the sample length, the absorption coefficient is then given by,

$$\frac{I}{I_o} = e^{-\mu(e)\bullet L} \qquad (2)$$

Or more commonly for transmittance,

$$\mu(e)L = \ln(I_o / I) \qquad (3)$$

And for fluorescence analysis this can be equivalently expressed as,

$$\mu(e)L = (I_f / I_o) \qquad (4)$$

Depending on the state of the solid sample, $\mu(e)$ can be measured in a variety of ways. The most common technique is the transmission mode for concentrated homogenous material. In this method, the energy dependent absorption coefficient is determined by measuring the intensity transmitted through the sample. For dilute thin films on substrates, fluorescence and electron yield measurements are widely used. Fluorescence emission, or the emission of other electrons (i.e. Auger electrons), occurs when higher-level electrons fill the excited core hole that was described above. The model in this report will examine the surface sensitivity of electrons excited and emitted through fluorescence emission.

Sudden jumps in the absorption coefficient signal these electron excitations. The data above these jumps exhibit oscillatory structure and has been named the X-ray absorption fine structure (XAFS). The absorption coefficient can be related to these XAFS oscillations $\chi(k)$ by,

$$\chi(k) = \frac{\mu(k) - \mu_o(k)}{\Delta\mu_o(k)} \qquad (5)$$

where $\mu(k)$ is the measured absorption coefficient subtracted from the smooth "bare atom" background, $\mu_o(k)$, and then divided by the "edge step" jump $\Delta\mu_o(k)$. This edge step is the normalization function, which is the absorption due to all processes that do not include the photoelectron backscattering effect.

The electron excitation can be seen as two different photoelectron waves. The first wave is the outgoing photoelectron wave leaving the absorbing atom and the second wave is the scattered wave returning from the neighboring atoms. Oscillations in the absorption coefficient are primarily due to the interference effect between the first outgoing wave function with the second wave function returning from neighboring scatter effects. By viewing the emitted electron as a propagating photoelectron wave (k) rather than a particle; and by assuming that only a single scatter occurs for every excited photoelectron wave, the XAFS equation can be simply modeled as the sum of two spherical sine waves,

$$\chi(k) = \frac{N_j \cdot S_o^2 \cdot F_j(k) \cdot e^{-2R_j/\lambda(k)} \cdot e^{-2\sigma_j^2 k^2}}{kR_j^2} \sin[2kR + \delta(k)] \qquad (6)$$

where the amplitude factor A_j is given by,

$$A_j(k) = \frac{1}{kR_j^2} S_o^2 \cdot F_j(k) \cdot e^{-2R_j/\lambda(k)} \cdot e^{-2\sigma_j^2 k^2} \qquad (7)$$

N_j is the number of equivalent atoms in shell j, S_o^2 is the amplitude reduction factor representing central atom shake-up and shake-off that accounts primarily for the many

body effects, which reduces the XAFS oscillation amplitude. $F_j(k)$ is the backscattering amplitude of the photoelectron off neighbor's j including a reduction due to the mean-free path of the photoelectron. $\delta_j(k)$ expresses the electronic phase shift due to the atomic potentials of both the central and the backscattering atoms, $\square^2$ is the corresponding mean-square relative displacement, and $\lambda(k)$ is the photoelectron mean free path.

The amplitude factor and phase shift for the Cd K-edge were extracted using the known structural data from the CIS spectra. The *ab initio* multiple-scattering code FEFF8 was used to calculate $F_j(k)$, $\delta_j(k)$, and $\lambda(k)$ for Cd K-edge data analysis [Ankudinov *et al.*, 1995].

3.3.2 XAFS spectrum

The single-electron excitations created by the photoelectric effect are the main features in an X-ray absorption spectrum. These excitations appear as sudden jumps in the absorption coefficient. XAFS spectroscopy measures the modulation of the X-ray absorption coefficient with respect to photon energy. An X-ray absorption spectrum of the CdSe standard is shown in Figure 3.3.2.1. When this energy reaches the binding energy specific to the atom of interest (i.e. the absorbing atom), a sharp increase is observed which is referred to as the absorption edge. This is where a core-level electron becomes promoted and is emitted out of the absorbing atom as a photoelectron. The atom is now left in an excited state with an empty electronic level, a core hole. The two areas extending past the absorption edge show various oscillations caused by interference from neighboring atoms with the ejected photoelectron.

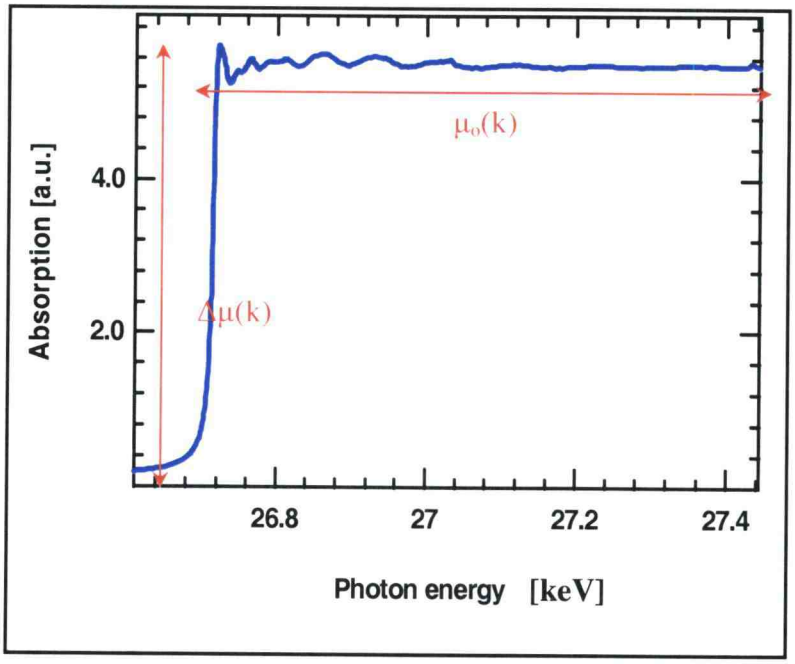

Figure 3.3.2.1: Raw XAFS data of CdSe standard

These oscillations will tell something about neighboring atoms. The first region is called the XANES (from 10 eV below E_o to about 30 eV above), which contains information on the electronic structure and geometrical configuration of the material. The second region describes local structure around the excited atom and is called the XAFS region (from 30 eV to 1000 eV above absorption edge).

3.3.3 Data Reduction

Standard methods and procedures were used to change the raw data into the normalized XAFS data that can then be interpreted according to the usual theoretical formulations [Sayers, 1987]. This was done using the WinXAS software package [Ressler, 1997]. Experimental intensity data with respect to photoelectron energy were first converted to absorption coefficient based on the intensities of the incident and

[Ressler, 1997]. Experimental intensity data with respect to photoelectron energy were first converted to absorption coefficient based on the intensities of the incident and transmitted beams. The resultant absorption spectra are subsequently subjected to pre-edge background removal when using an ionization detector. However, the MED detector eliminates this step as described in the section above. The next step was to convert the photon energy $\boldsymbol{E}$ to the photoelectron wave vector $\boldsymbol{k}$ via,

$$k = \sqrt{2m(E - E_o)/h^2} \qquad \textbf{(8)}$$

Where m is the electron mass, and E_o is the K-edge energy. The normalized XAFS spectra were obtained by subtracting the background from the measured absorption coefficient and are then converted by the edge energy jump. A typical Cd K-edge spectrum of $CuInSe_2$ is shown in Figure 3.3.3.1.

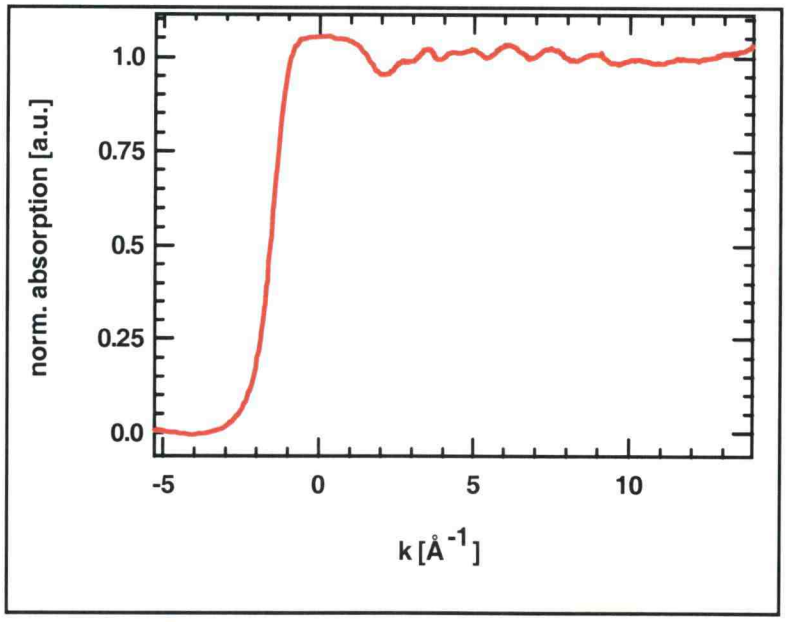

Figure 3.3.3.1: Normalized XAFS spectra of CdSe standard

"knots" where the polynomials meet. The danger in using too many knots is that the spline may have enough degrees of freedom to follow the XAFS oscillations. In addition, the use of too few knots can interfere with later analysis of the fine structures in the spectra. The number of splines used in our mue fit was five, and the resulting $\chi(k)$ oscillations are shown in Figure 3.3.3.2.

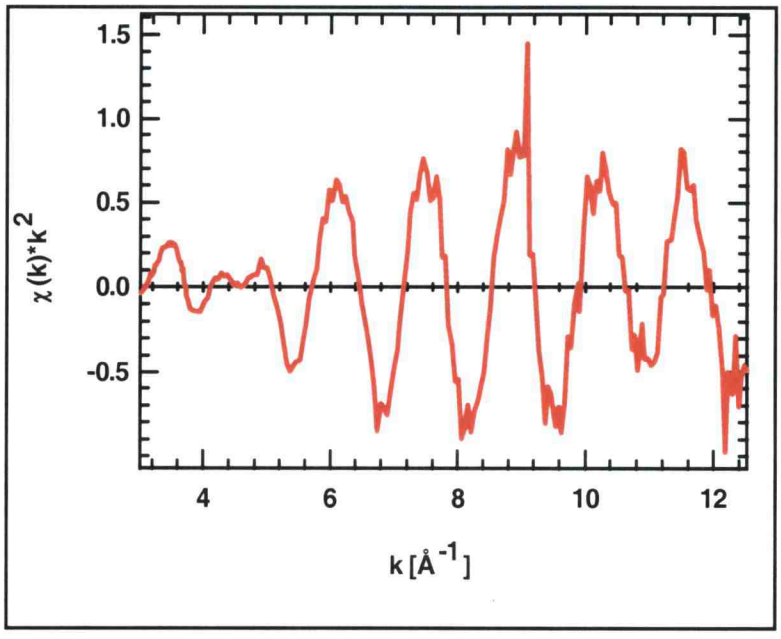

Figure 3.3.3.2: Cd K-edge XAFS oscillations of CdSe Standard

A Gaussian window between 3.5-12.5 $Å^{-1}$ was used for Fourier transforms. The analysis was not sensitive to types of windows when we analyzed the standard compound and the unknown under exactly the same conditions. This data was then Fourier transformed into real space. The Fourier-transformed (FT) Cd K-edge R-space data are shown in Figures 3.3.3.3 and 3.3.3.4.

transformed (FT) Cd K-edge R-space data are shown in Figure 3.3.3.3. The resulting first shell EXAFS spectrum is shown in Figure 3.3.3.4. The same k and r-space windows were applied to the data analysis for the spectra of CIS.

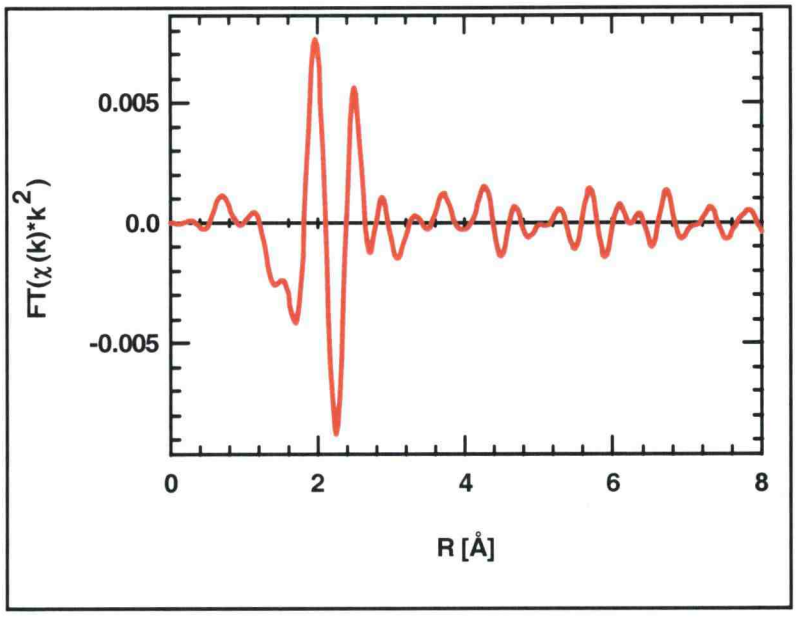

Figure 3.3.3.3: Imaginary part of the Fourier transform of Cd K-edge of CdSe

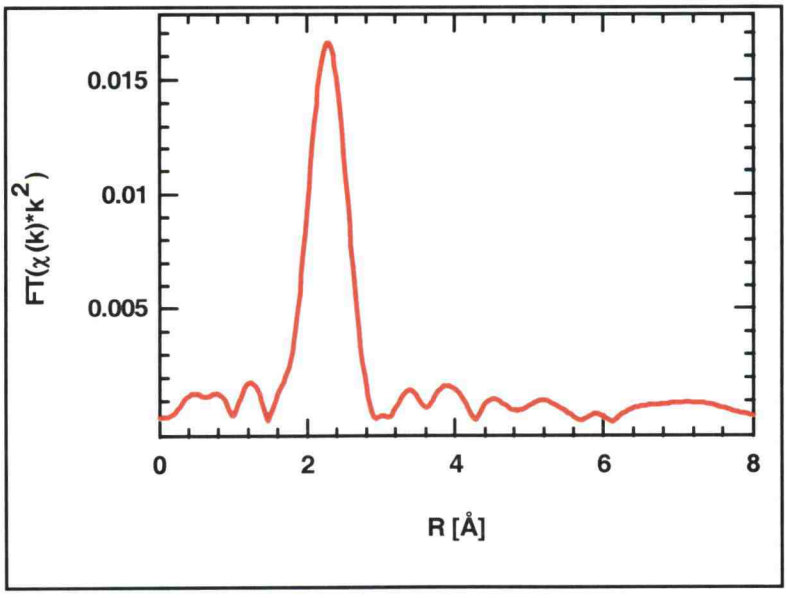

Figure 3.3.3.4: The magnitude of the Fourier transform in r-space of CdSe

Chapter 4

Results and Discussion

This chapter is divided into three sections involving the data acquired from the X-ray absorption fine structure experiments described in Chapter 3. First, the EXAFS spectra of the CdSe, $Cd(OH)_2$, and $CdIn_2Se_4$ standards are used to compare with the EXAFS data of the CIGS/Cd PE treated thin films. Next a least-square fitting was performed on the resulting EXAFS data of the CIGS/Cd PE treated thin films using theoretically calculated standards produced with two different crystal models. In the last section, X-ray Photoelectron Spectroscopy (XPS) results will be discussed.

4.1 Comparison of EXAFS Spectra of CdSe, $Cd(OH)_2$, $CdIn_2Se_4$ and CIGS/Cd PE treated samples

Pure powder $CdIn_2Se_4$ samples were studied and compared with the CdSe powder standard. In Figure 4.1.1.1b, the Cd-Se bond length for $CdIn_2Se_4$ is the same as the CdSe standard sample, however, the numbers of first nearest neighbors differ. The main peak corresponds to Cd-Se interactions, which is consistent with first principle calculations of published earlier [Zunger *et al.*, 1988].

Figure 4.1.1.2a illustrates the oscillatory χ function of the Cd *K-edge* in the CIGS/Cd 15PE sample. Fourier transforming this wave data isolates these characteristic fluctuations and expresses the data in *r* space, shown in Figure 4.1.1.2b.

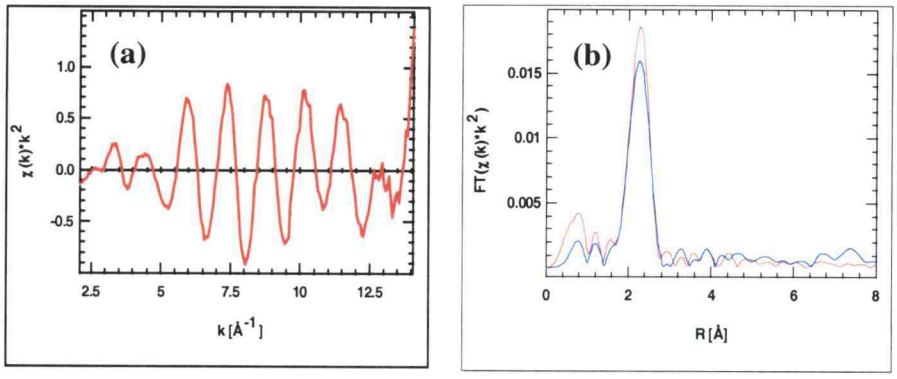

Figure 4.1.1.1: Cd K-edge EXAFS χ functions, (b) Fourier transform of Cd *K*-edge of $CdIn_2Se_4$ powder samples (red) and CdSe powder (blue) for comparison.

The main peak at 2.1 Å corresponds to a Cd^{2+} complex with another species within the absorber. In addition, this signal is coupled along with a distinct shoulder peak roughly 0.3 Å lower than the main peak. This suggests another interaction present in addition to the Cd-Se bond.

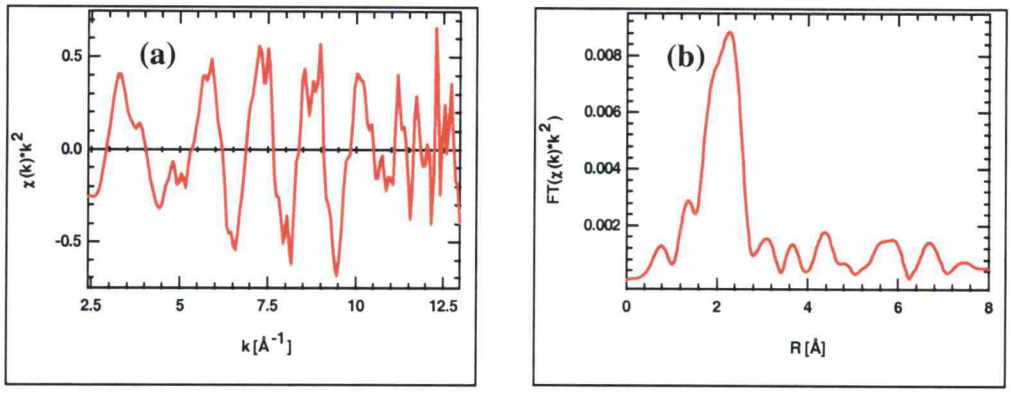

Figure 4.1.1.2: (a) Cd *K-edge* EXAFS χ function, (b) Fourier transform of Cd *K*-edge of CIGS/Cd PE at 1.5 M $CdCl_2$

Comparing the spectra of these transformed data with CdSe and CdO standards suggests these peaks may be Cd-Se and Cd-O bonds. Figure 4.1.1.3 superimposes the EXAFS spectra of CdSe standard with the two PE treated samples. The main peaks at

~2.1 Å of the PE treated samples are consistent with the Cd-Se bonds. The intensities however are noticeably dissimilar in all three samples, indicating that there is a difference in the average of the nearest neighbor numbers between these samples. Figure 4.1.1.4 is the comparison of the CdO EXAFS spectra with the two PE treated samples.

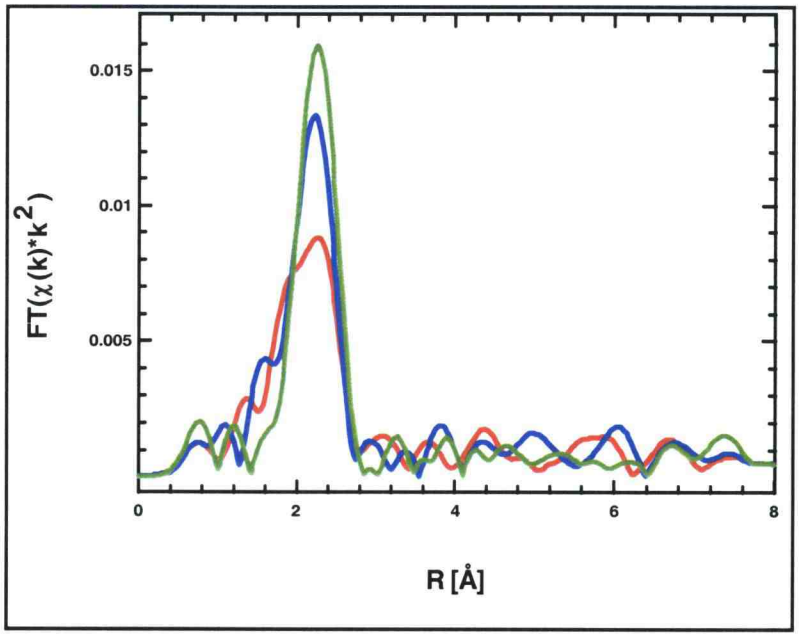

Figure 4.1.1.3: Fourier transforms of Cd K-edge EXAFS χ(k) functions on CdSe and treated samples of CIGS thin films (green line represents CdSe, blue line is CIGS/Cd 0015PE, and the red line is CIGS/Cd 15PE)

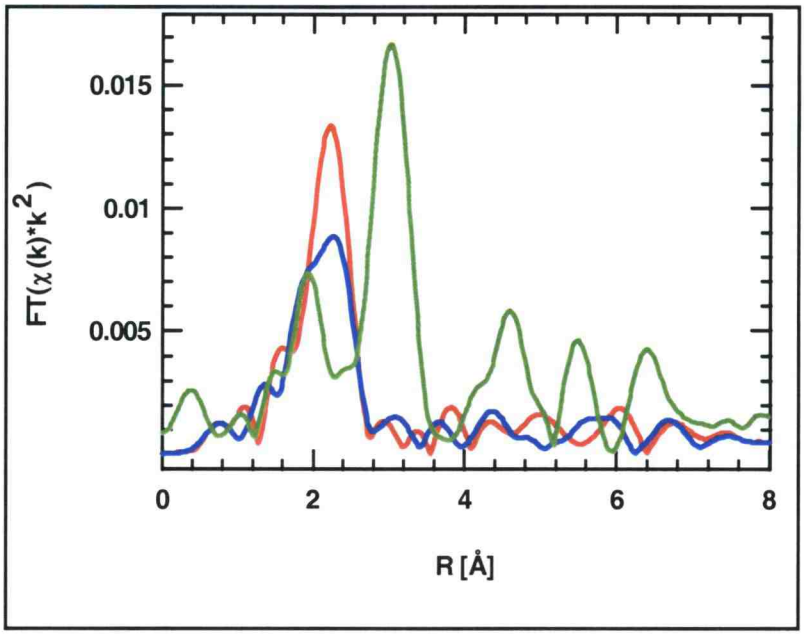

Figure 4.1.1.4: Fourier transforms of Cd K-edge EXAFS χ(k) functions on CdO and treated samples of CIGS thin films (green line represents $Cd(OH)_2$, blue line is CIGS/Cd 0015PE, and the red line is CIGS/Cd 15PE).

The peak at ~1.9 Å in Figure 4.1.1.4. for the CdO spectrum (green) corresponds to the Cd-O bonds, which matches well with the shoulder peak. This suggests that the shoulder peak represents Cd-O bonds. Theoretical standard were created from crystallography data reported in previous literature. This will be described in the next section of the least-square fitting analysis.

4.2 Least-square fits

In order to obtain more quantitative details about the local environment around the cadmium atoms, a least-square fitting was performed using the theoretical standards calculated from the multiple scattering paths code FEFF8.

We fit the FT of $k\chi(k)$ with a k weighting of 2. This reduces the effect of overlapping peaks [Hayes, 1982]. $F_j(k)$, $\delta_j(k)$, and $\lambda(k)$ were calculated using FEFF8. The information for each path is called a "standard". The data are fit to a sum of theoretically calculated standards, which include all single-scattering paths. Other multiple-scattering paths were neglected. Only the first shell scattering effects were considered in this study.

Several of the parameters were constrained in order to decrease the number of fitting parameters. Since measurements of S_o^2 and N_i are correlated, we performed a fit where the N_i was fixed to four and resulting in a value of S_o^2=0.94, and was used for all fits to the cadmium treated CIGS samples. Figure 4.2.1.1 shows the least-square fit to the CIGS/Cd 15PE sample using a one-phase model described in the following section.

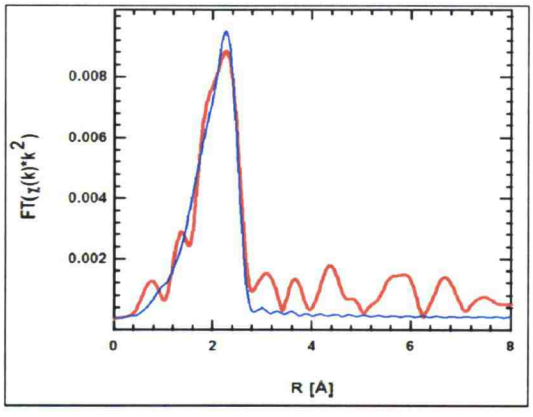

Figure 4.2.1.1: Least square fits of the Fourier transformed CIGS:Cd 15PE first shell of the one phase model

This model was created by implanting a cadmium ion in the [0.5, 0, 0.25] copper site, and also an oxygen ion in the [0.22, 0.25, 0.5] selenium site. The crystal structure was generated by using Carine Crystallography software, and the Cd local structure was applied in the calculation of scattering paths in FEFF8. The fitting results of the one phase

model are shown in Table 4.2.1.1. It appears that, based on our initial model, the least-square fitting results are not consistent with the model since the nearest neighbor representing the Cd- Se is still 4. It is expected that the sum of the first nearest neighbors should be around 4 for tetrahedrally bonded cadmium atoms. However, from this first model fit, the total first nearest neighbor number is high at 9.41. Therefore a second model was formulated to fit the CIGS:Cd 15PE treated sample.

	Coordination Number	Bond Length (Å)	σ^2(Å^2):	S_0^2:
Cd-K edge	5.41	R_{Cd-O} 2.33	$2.83X10^{-2}$	0.94
	4	R_{Cd-Se} 2.62	$8.43X10^{-3}$	0.94

Table 4.2.1.1: Atomic parameters from first model fit of CIGS:Cd 15PE

The second model consisted of the same implanted cadmium ion on the copper site, with the addition of five oxygen atoms now evenly distributed around the cadmium. This simulated the combination of the tetrahedrally bonded Cd-Se interaction in CIS:Cd and the octahedrally bonded Cd-O bonds in pure compound as illustrated in Figure 4.2.1.2.

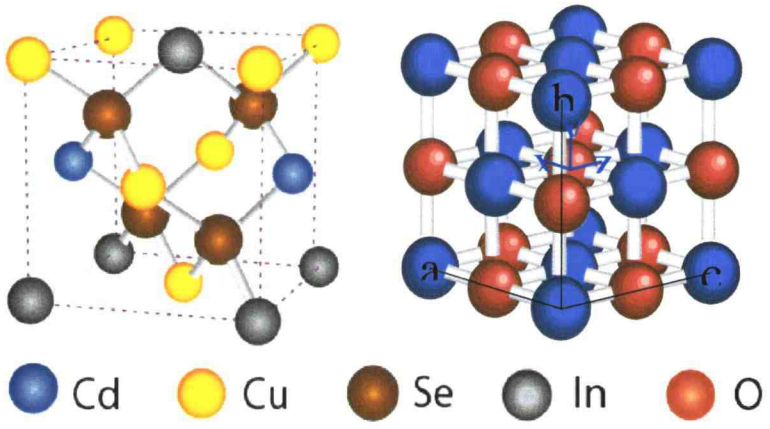

Figure 4.2.1.2: Crystal structure of Cd-Se in CIS and Cd-O compound interactions

A combination of the two structures was made with the aide of the Carine Crystallography software by adding five oxygen atoms around the cadmium atom in CIGS following the octet rule. The fit using the second model is shown in Figure 4.2.1.3 and the results are listed in Table 4.2.1.2.

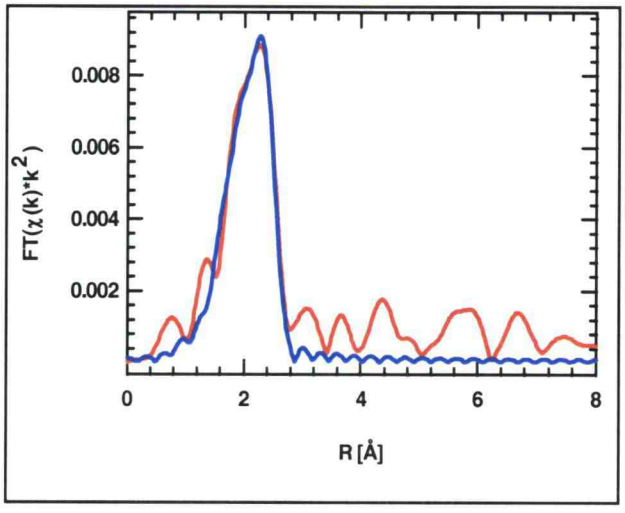

Figure 4.2.1.3: Least-square fits of the Fourier transformed CIGS:Cd 15PE first shell of the two phase model

	Coordination Number	Bond Length (Å)	σ^2(Å^2):	S_0^2:
Cd-K edge	6.07	R_{Cd-O} 2.33	$3.03X10^{-2}$	0.94
	4.03	R_{Cd-Se} 2.62	$8.44X10^{-3}$	0.94

Table 4.2.1.2: Atomic parameters from second model fit of CIGS:Cd 15PE

The fit of these results is better than that of the first model as shown in Figure 4.2.1.1. While the sum of the total first nearest neighbor around the cadmium atom is still too high

at NN_{Cd}=10.1. This may be due to the Cd-O and Cd-Se peaks being allowed to vary over too broad a range. Such variation would cause the least-square fitting to fall into a false minimum in the fitting parameter such that the data may be affected [Stern *et al.*, 1993]. Further constraining parameters to each scattering path to known physical factors would limit the unusual errors observed in the local minimization least-square fit.

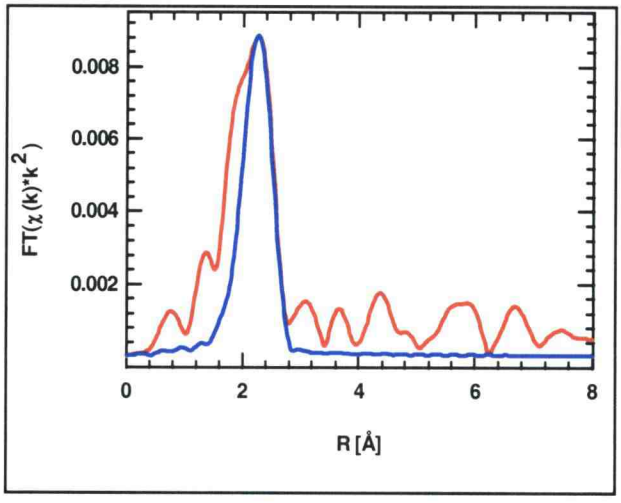

Figure 4.2.1.4: CdSe structure fit with CIGS/Cd 15PE treatment (NN=2.3, S_o^2=0.94, R=2.63 Å)

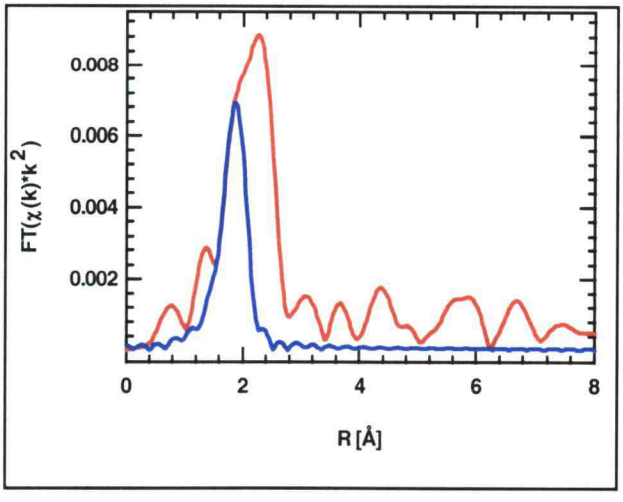

Figure 4.2.1.5: CdO structure fit with CIGS/Cd 15PE treatment (NN=1.9, S_o^2=0.94, R=2.33 Å)

The diagrams shown in Figures 4.2.1.4 and 4.2.1.5 represent the calculated first shell CdSe and CdO EXAFS spectra compared with the CIGS:Cd 15PE. This was done by fixing the distances, mean-square relative displacement, and energy shift parameters of Cd and O/Se bonds in the standards. Based on these results a fit taking these constraints into account with the two phase model was regenerated (see Figure 4.2.1.6). The resulting data is given in Table 4.2.1.3.

The standard fit is very well matched with the data and the total nearest neighbor number is consistent with the model at NN=4.2 at the main peak suggesting the cadmium interaction is dominated by the Cd-Se bond. In addition there is also Cd-O bonding identified at 1.4 nearest neighbors in the first shell of the CIS absorber.

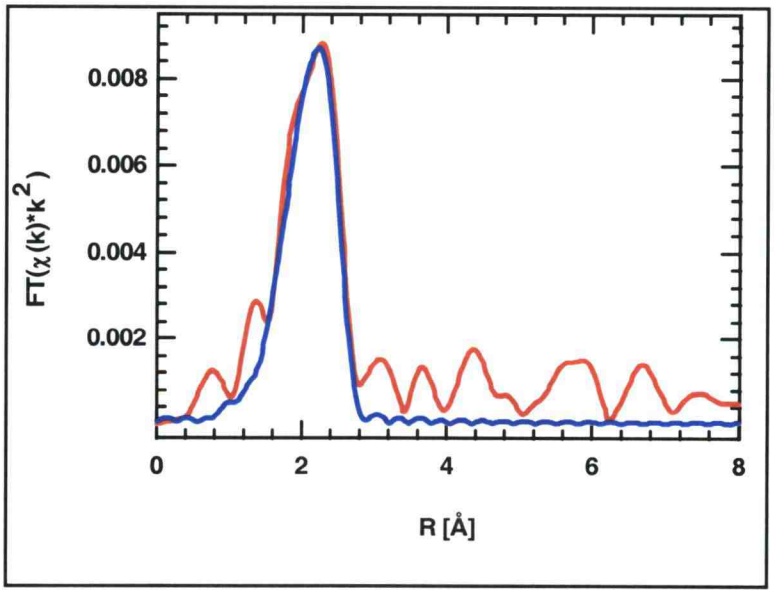

Figure 4.2.1.6: Least square fits to the Fourier-filtered CIGS:Cd 15PE first shell *k*-weighted χ(k) for parameterized two phase model

	CIS:1.5 M Cd	Standards
S_0^2:	0.94	0.94
	Cd-Se	**Cd-Se**
NN:	2.3	4
R_{Cd-Se}(Å):	2.63	2.63
σ^2(Å^2):	5.50E-03	5.51E-03
	Cd-O	**Cd-O**
NN:	1.9	6
R_{Cd-O}(Å):	2.33	2.33
σ^2(Å^2):	5.50E-03	8.20E-03

Table 4.2.1.3: Atomic parameters for CIS/Cd 15PE theoretical fitting results Compared with CdO and CdSe standards

A fit taking these constraints into account with the two phase model was also generated for the lower concentrated sample, CIS/Cd 0015PE. The same individual fits of pure CdO and CdSe is shown in Figure 4.2.1.7 and 4.2.1.8. The resulting data was used in the two phase model as described above and fitted to the CIS/Cd 0015PE collected data. The fit is given in Figure 4.2.1.9 and the results given in Table 4.2.1.4.

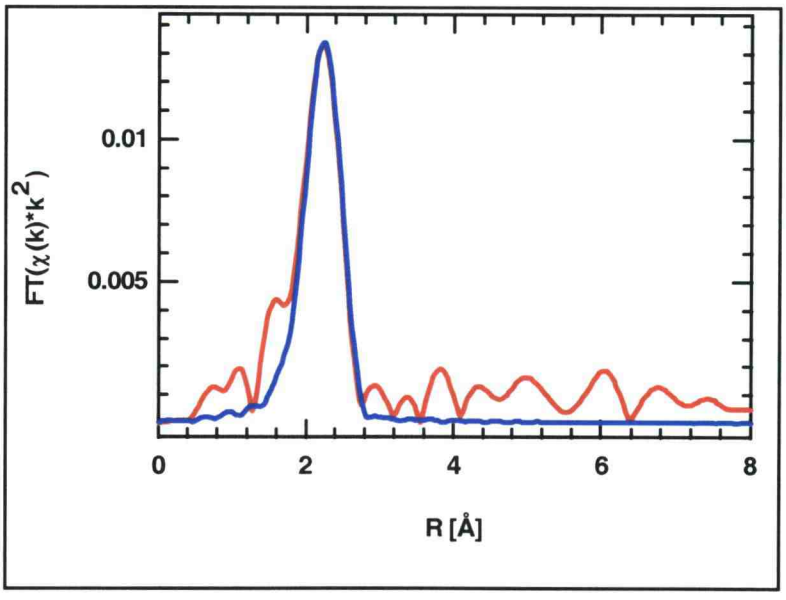

Figure 4.2.17: CdSe structure fit with CIGS/Cd 0015PE treatment (NN=3.5, S_o^2=0.94, R=2.63 Å)

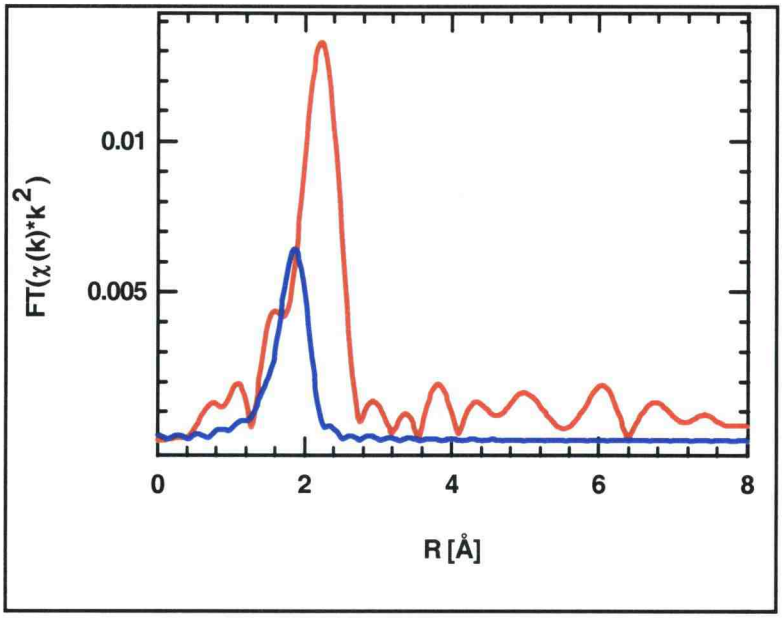

Figure 4.2.1.8: CdO structure fit with CIGS/Cd 0015PE treatment (NN=0.5, S_o^2=0.94, R=2.33 Å)

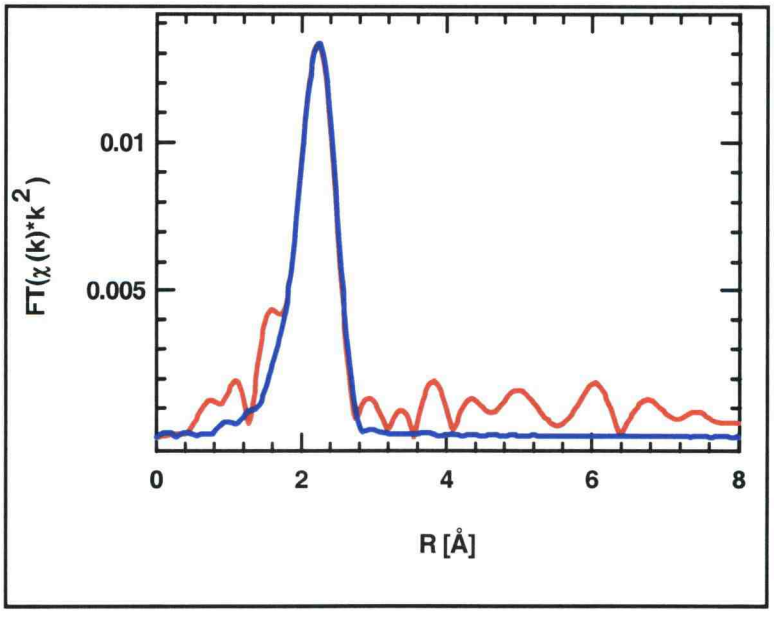

Figure 4.2.2.9: Least square fit to the Fourier-filtered CIGS:Cd 0015PE two phase with Cd-O R=2.33 Å, NN= 0.5 and Cd-Se NN=3.5

	CIS:1.5 M Cd	Standards
S_0^2:	0.94	0.94
	Cd-Se	Cd-Se
N:	3.5	4
R_{Cd-Se}(Å):	2.63	2.63
σ^2(Å^2):	5.50E-03	5.51E-03
	Cd-O	Cd-O Standard
N:	0.5	6
R_{Cd-O}(Å):	2.33	2.33
σ^2(Å^2):	5.50E-03	8.20E-03

Table 4.2.1.4: Atomic parameters for CIS/Cd 0015PE theoretical fitting results Compared with CdO and CdSe standards

4.3 X-ray Photoelectron Spectroscopy (XPS)

The two phase model described above is validated through the X-ray Photoelectron Spectroscopy technique. Figure 4.3.1.1 is a XPS spectrum of the Cd $3d^{3/2}$ shell that is present in the PE treated CIGS thin film.

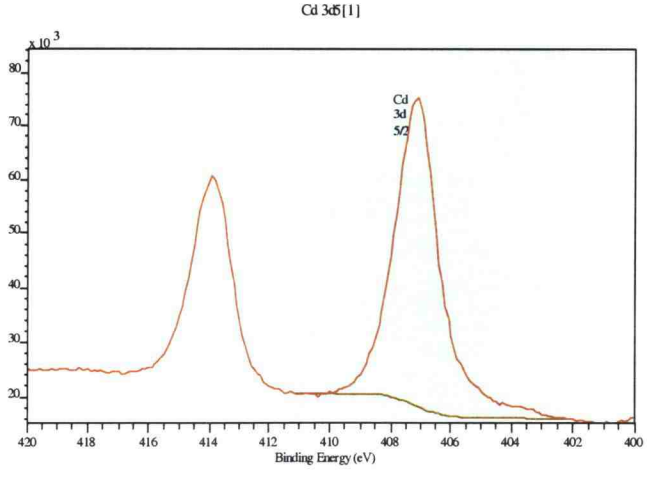

Figure 4.3.1.1: XPS analysis of #1852 CIGS sample

Name	Pos	At%
C	287.4	60.12
O	534.1	26.84
Cd	407.7	13.04

Table 4.3.1.1: Atomic percentage of CIGS/Cd 15PE as is sample

Table 4.3.1.1 shows the surface atomic concentration in the PE treatment of the surface in CIGS/Cd 15PE thin films. The high carbon and oxygen concentrations are due to CO_2 and O_2 contamination from exposure to the atmosphere. Table 4.3.1.2 shows the atomic percentage of the constituent atoms in the CIGS/Cd 15PE sample after argon surface cleaning to clear the thin film of carbon and oxygen contamination from atmospheric exposure. Cadmium ions are again present with the inclusion of copper, indium, selenium, and gallium atomic percentages.

Name	Pos	At%
Se	56.8	25.45
Cd	407.1	24.93
O	531.9	22.03
In	446.6	7.276
Cu	933.5	7.158
C	286.8	7.003
Zn	1022.5	3.114
Ga	1118.3	3.032

Table 4.3.1.2: Atomic percentage of CIGS/Cd 15PE argon cleaned sample

Some zinc was detected, though this can be linked to contamination of the XPS sample chamber from previous uses. A charge balance of the ions present was done considering Cd-Se interactions and confirmed that some oxygen is available for interaction with cadmium cations. This also substantiates the nominal composition as $CuIn_{0.7}Ga_{0.3}Se_2$.

Chapter 5

Conclusions and Recommendations for Future Study

5.1 Conclusions

EXAFS analysis of CIGS thin films treated with two differing concentrations of the Cd partial electrolyte is consistent with a two phase model. The model used in this study was generated from crystal structures consisting of CdSe tetrahedron and CdO octahedron in the CIGS lattice. Cd-Se and Cd-O bonds were found to be the main interaction of the Cd atom in the CIS/Cd PE treated samples. This was determined by comparing the CIGS/Cd PE EXAFS spectra to the EXAFS spectra of CdSe and CdO standards. The higher concentrated treatment has more Cd-O first nearest neighbors, while the lower concentrated sample has more Cd-Se nearest neighbors.

5.2 Recommendations for Future Study

The deposition of Cd^{2+} window layer via wet chemistry depends on the reaction conditions. Thus, further study is needed in several areas. Some suggestions are listed below.

- Additional standard correlations maybe further investigated.
- More extensive XAFS grazing incident experiments with CIGS/Cd PE samples.

- The concentration variation of Cd complex formations, i.e., the conversion of $Cd(OH)_2$ solids, until the entire solid is either eliminated needs to be investigated.
- To find a simple kinetics expression for this reaction, the additional experiment with varying reactant concentration should be performed.
- Further study to find a method to determine the extent of conversion of each O and Se graded distribution is needed.

Bibliography

1. A. L. Ankudinov and J. J. Rehr, Phys. Rev. B 52, 2995 (1995).

2. M.I. Boyanov, S.D. Kelly, K.M. Kemner, B.A. Bunker, J.B. Fein, and D.A. Fowle, "Adsorption of Cadmium to B. subtilis Bacterial Cell Walls - a pH-Dependent XAFS Spectroscopy Study", accepted for publication in *Geochimica et Cosmochimica Acta* (2003).

3. F. Bridges, C. H. Booth, and G. G., Physica B 208 & 209, 121 (1995)

4. C. -H. Chang, S. –H. Wei, J. W. Johnson, R. N. Bhattacharya, B. J. Stanbery, T. J. Anderson, and R. Duran, Jpn. J. Appl. Phys., Suppl. 39-1, 411 (2000).

5. C. -H. Chang, S. –H. Wei, J. W. Johnson, B. Zhang, N. Leyarovska, G. Bunker, and T. J. Anderson, Phys. Rev. B, 68, 054108-1 (2003)

6. M.A. Contreras, B. Egaas, K. Ramanathan, J. Hiltner, A. Swartzlander, F.Hasson, and R. Noufi, Prog. Photovoltaics 7, 311 (1999).

7. T.K. Eccles, Ph.D. thesis, Standford University, 1977. (Available as SSRL Report No 78/01.)

8. S. M. El-Mashri. Journal of Materials Science Letters, 7(4), (1988), 345-6.

9. A. Gabor et al., "High-efficiency CuInxGa1-xSe2 Solar Cells Made from (Inx,Ga1-x)2Se3 Precursor Films", Appl. Phys. Lett. 65, 1994, pp. 198-200.

10. T. M. Hayes and J. B. Boyce, in Solid State Physics, edited by H. Ehrenreich, F. Seitz, and D. Turnbull (Academic, New York, 1982), Vol. 37, p. 173.

11. C. Heske *et al.* Appl. Phys. Lett. 74, 1451 (1999).

12. P. Johnson et al., "Interface Properties of CIGS/Buffer Layers Formed by the Cd-Partial Electrolyte Process", 29th IEEE PVSC, 2002.

13. J. Kessler, K.O. Velthaus, M. Ruckh, R. Laichinger, H.W. Schock, "Chemical Bath Deposition of CdS on $CuInSe_2$, Etching Effects and Growth Kinetics", proc. 6th Int. PVSEC, New Delhi, India, pp.1005, 1994.

14. S. Kim, Y.L. Soo, G. Kioseoglou, and Y.H. Kao, "Compositional Intermixing at CdS/Cu(In,Ga)Se_2 rough interface study by x-ray fluorescence", American Institute of Physics, pp. 6416-6423, 2002.

15. G. G. Li, F. Bridges, and C. H. Booth, Phys. Rev. B, 52, 6332 (1995).

16. S. Licht, "High Efficiency Solar Cells: What are the highest solar energy conversion efficiencies?", The Electrochemical Society Interface, pp.34-39, 1997.

17. F. W. Lytle *et al.*, Nucl. Instrum. Meth., 226, p.542 (1984).

18. K. I. Pandya and D. C. Koningsberger. "Analysis of Microelectronics Materials and Devices", (1991), 637-655.

19. K. Ramanathan, R. N. Bhattacharya, J. Granata, J. Webb, D. Nieles, M. A. Contreas, H. Wiesner, F.S. Hasoon, and R. Noufi, Proceeding of the 26th IEEE Photovoltaic Specialists Conference, Anaheim, CA (IEEE, New York, 1997, p. 319.

20. K. Ramanathan, H., Wiesner, S. Asher, D. Niles, R.N. Bhattacharya, J. Keane, M.A. Contreras, and R. Noufi, "High Efficiency Cu(In,Ga)Se_2 Thin Film Solar Cells Without Intermediate Buffer Layers", 2nd WCPEC Vienna, pp.477-481, 1998.

21. T. Ressler, J. Physique IV, 7 C2-269 (1997).

22. D. Sayers and B. Bunker, "X-ray Absorption: Principles, Application, Techniques of EXAFS, SEXAFS, and XANES, edited by D.C. Koningsberger and R. Prins (Wiley, New York, 1987), Chap. 6.

23. T. Shibata, H. Tostmann, B. Bunker, A. Henglein, and D. Meisel, "XAFS Studies of Gold and Silver-Gold Clusters in Aqueous Solutions", Proceedings of the 11th International Conference on X-ray Absorption Fine Structure (XAFS XI), July 27-31, 2000 in Ako city, Japan, *J. Synch. Radiation*, **8**, 545-547 (2001).

24. T. Shibata, B. A. Bunker, Z. Zhang, D. Meisel, C. F. Vardeman, and J. D. Gezelter, "Size Dependent Spontaneous Alloying of Au-Ag Nanoparticles", *J. Am.Chem. Soc.* **124**, 11989-11996 (2002).

25. T. Shibata, B.A. Bunker, J.F. Mitchell, and P.Schiffer, "Indications of intrinsic chemical and structural inhomogeneity in lightly doped $La_{1-x}Sr_xMnO_3$", *Phys. Rev. Lett.*, **88**, 207205 (2002).

26. Z.A. Shukri, C. H. Champness, and I. Shih, J. Cryst. Growth, 129, 107 (1993).

27. Y. L. Soo, S. Huang, Y.H. Kao, S.K. Deb, K. Ramanathan, and T. Takizawa, "Migration of Constituent Atoms and Interface Morphology in a Heterojunction

Between CdS and $CuInSe_2$ Single Crystals", J. Appl. Phys., 86, pp.6052-6058, 1999.

28. Y. L. Soo, S. Huang, S. Kim, G. Kioseoglou, and Y. H. Kao, "Effects of heat treatment on diffusion of Cu atoms into CdTe single crystals", Appl. Phys. Lett., 76, 25, pp.3729-3731.

29. E. A. Stern, M. Quian, Y.L Yacoby, S. M. Heald, and H. Maeda, Physica C, 209, 331 (1993).

30. S. –H. Wei and H. Krakauer, Phys. Rev. Lett. 55, 1200 (1985), and references there in.